CASL A DOE Energy Innovation Hub

SAND2018-10504R
CASL-X-2018-XXXX

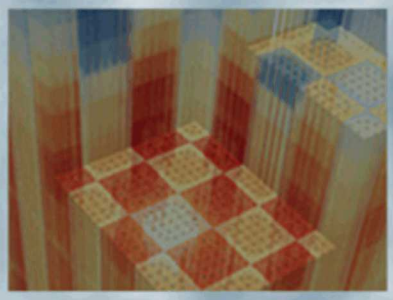

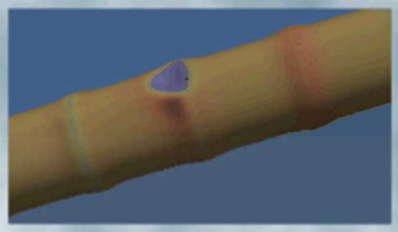

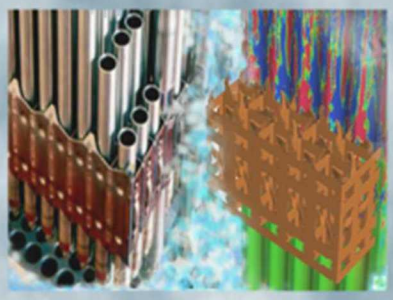

Average Surface Mapping Model Calibration

L3:THM.DEMO.P17.01

Natalie Gordon, Sandia National Laboratories

September 17, 2018

Sandia National Laboratories is a multimission laboratory managed and operated by National Technology and Engineering Solutions of Sandia, LLC, a wholly owned subsidiary of Honeywell International, Inc., for the U.S. Department of Energy's National Nuclear Security Administration under contract DE-NA0003525. SAND2018-XXXXXXXX

Sandia National Laboratories

U.S. DEPARTMENT OF ENERGY | Nuclear Energy

REVISION LOG

Revision	Date	Affected Pages	Revision Description
0		All	Initial Release

Document pages that are:

Export Controlled _____

IP/Proprietary/NDA Controlled_____

Sensitive Controlled_____

Requested Distribution:

To:

Copy:

EXECUTIVE SUMMARY

This milestone presents a demonstration of an average surface mapping model that maps single-phase average wall temperatures from STAR-CCM+ to Cobra-TF using a multiplier that is linearly dependent on axial and azimuthal coordinates of the Cobra-TF mesh. The work presented herein lays the foundation for adding greater complexity to the average surface mapping model such as fluid property dependence. This average surface mapping model will be incorporated into the surface mapping model developed by Lindsay Gilkey to map fluctuations from the mean surface temperatures.

CONTENTS

LIST OF FIGURES

LIST OF TABLES

ACRONYMS

CASL	Consortium for Advanced Simulation of Light Water Reactors
CFD	computational fluid dynamics
CTF	COBRA-TF subchannel thermal-hydraulics code
DOE	US Department of Energy
FA	Focus Area
Hi2Lo	High-to-Low
SNL	Sandia National Laboratories
STAR	STAR-CCM+ CFD code
THM	Thermal Hydraulic Methods
UQ	uncertainty quantification
V&V	verification and validation
VVI	Verification and Validation Implementation
VVUQ	Verification, Validation and Uncertainty Quantification
WEC	Westinghouse Electric Company

NOMENCLATURE

A	Area
c_p	Specific Heat
h	Heat transfer coefficient
h_{CTF}	CTF heat transfer coefficient
$h_{CTF-pre}$	CTF heat transfer coefficient calculated from CTF output
h_{STAR}	STAR heat transfer coefficient
$\dot{m}$	Mass Flow Rate
m_o^*	User-defined input to generate manufactured solution for M
m_1^*	User-defined input to generate manufactured solution for M
m_2^*	User-defined input to generate manufactured solution for M
M	Multiplier used in the surface average mapping model
M_0	Constant coefficient in the surface average mapping model multiplier
M_1	Linear Taylor series describing azimuthal dependence of M
M_{10}	Constant coefficient of the linear azimuthal dependence of M
M_{11}	Coefficient of azimuthal mass flow rate dependence
M_{12}	Coefficient of azimuthal Reynolds number dependence
M_{13}	Coefficient of azimuthal Prandtl number dependence
M_{14}	Coefficient of azimuthal linear heat rate dependence
M_{15}	Coefficient of azimuthal inlet temperature dependence
M_2	Linear Taylor series describing axial dependence of M
M_{20}	Constant coefficient of the linear axial dependence of M
M_{21}	Coefficient of axial mass flow rate dependence
M_{22}	Coefficient of axial Reynolds number dependence
M_{23}	Coefficient of axial Prandtl number dependence
M_{24}	Coefficient of axial linear heat rate dependence
M_{25}	Coefficient of axial inlet temperature dependence
$M_{exact,MMS}$	Analytical manufactured solution for M
$M_{o,exact,MMS}$	Analytical manufactured solution for M_0
$M_{10,exact,MMS}$	Analytical manufactured solution for M_{10}
$M_{20,exact,MMS}$	Analytical manufactured solution for M_{20}
$M_{exact,MMS,noise}$	Analytical manufactured solution for M with noise
ΔPr	Difference in Prandtl number
$\Delta q'$	Difference in linear heat rate
q'	Linear heat rate
q''	Heat flux
q''_{CTF}	Heat flux in CTF
q''_{STAR}	Heat flux in STAR
$\dot{Q}$	Core power
Q_{CTF}	Heat transfer in CTF
Q_{STAR}	Heat transfer in STAR
ΔRe	Difference in Reynolds number
θ	Azimuthal position in CTF coordinates
θ_o	Azimuthal reference point (0 radians)
$\Delta\bar{T}$	Difference in average temperature
$max\Delta\bar{T}$	Maximum difference in average temperature
ΔT_{in}	Difference in inlet temperature

T_{in}	Inlet temperature
$\bar{T}_f$	Average fluid temperature
$\bar{T}_{f,MMS}$	Average fluid temperature manufactured solution
$\bar{T}_{f,CTF}$	Average fluid temperature from CTF
$\bar{T}_{f,CTF,MMS}$	Average CTF fluid temperature manufactured solution
$\bar{T}_{f,STAR}$	Average fluid temperature from STAR
$\bar{T}_{f,STAR,MMS}$	Average STAR fluid temperature manufactured solution
T_w	Rod wall temperature
$\bar{T}_{w,CTF}$	Average wall temperature from CTF
$\bar{T}_{w,CTF,MMS}$	Average CTF wall temperature manufactured solution
$\bar{T}_{w,CTF-pre}$	Average wall temperature taken from CTF output
$\bar{T}_{w,CTF-post}$	Average CTF wall temperature after average surface mapping model applied
$\bar{T}_{w,STAR}$	Average wall temperature from STAR output
$\bar{T}_{w,STAR,MMS}$	Average STAR wall temperature manufactured solution
z	Axial position in CTF coordinates
z_o	Axial reference point (initial z)

1. MILESTONE DESCRIPTION

1.1 Introduction and Motivation

Prior to the work performed in this milestone, STAR-CCM+ (STAR) wall temperature mapping to COBRA-TF (CTF) was performed to specific boundary conditions and geometry. New STAR runs were required to create each wall temperature map whenever the geometry or boundary conditions were changed. The goal of this work is to construct a general model for mapping average surface temperatures from STAR to CTF that is not specific to boundary conditions or geometry. STAR runs will only be needed to generate the model initially, but would not be required within the boundary conditions in which the average surface mapping model was trained.

The previous 1:1 direct STAR-to-CTF map assumed no uncertainty and is time intensive since there is a map for each test. The average surface mapping model will carry uncertainty, but the model will be improvable through calibration and only one is needed for multiple experiments, unlike the direct map. The work described in this milestone report is the calibration of three coefficients in the average surface mapping model that depend only on rod θ and z. Confidence bounds on the surface mapping model will also be available through the calibration process.

The scope of this milestone is incorporating azimuthal and axial dependence in the average surface mapping model for a single channel demonstration problem. Follow-on work will include incorporating a globally applicable average surface mapping model that will contain fluid and flow property dependencies.

1.1.1 Milestone Tasks and Implementation

STAR and CTF runs were performed over a given set of boundary conditions for a single channel geometry [1]. This simplified geometry was chosen for the purposes of demonstrating the average surface mapping model and more realistic geometric complexity will be added in future work. Average surface temperatures from the rod and average fluid temperatures from the channel were post-processed from each code. The average surface mapping model was developed and then tested using synthetic verification data.

Deterministic calibrations using the verification data and the single channel demonstration data were performed using Dakota 6.7. Future work will include adding other dependencies to the average surface mapping model such as fluid properties. Once all the dependencies have been added, the average surface mapping model will be incorporated into the surface mapping model described in L3:PHI.CTF.P17.02.

1.2 Working Group and Ackknowledgements

The working group for this milestone consisted of Natalie Gordon (SNL), Lindsay Gilkey (SNL), Daniel Orea (SNL), Vince Mousseau (SNL), Bob Salko (ORNL), and Dave Pointer (ORNL).

A technical review of this report was performed by Vince Mousseau and Lindsay Gilkey.

2. SINGLE PHASE AVERAGE SURFACE MAPPING MODEL AND DESCRIPTION

2.1 Linear Average Surface Mapping Model Methodology

The average surface mapping model will assume uncertainty and a linear dependence on geometry parameters. This will be achieved through use of a multiplier between the heat transfer coefficient of STAR and CTF. The average surface mapping model assumes the following:

- the average bulk fluid temperature in STAR and CTF is equal for the same subchannel and z-position,
- the linear heat rate per rod is constant for each experiment,
- and the multiplier, M, is linearly dependent in the azimuthal (θ) and axial (z) directions.

2.1.1 Derivation of the Multiplier, M

The purpose of the surface map is to impart the amount of heat transfer calculated in STAR into CTF such that,

$$Q_{CTF} = Q_{STAR}$$

which decomposed is,

$$h_{STAR}A\left(\bar{T}_{w,STAR} - \bar{T}_{f,STAR}\right) = h_{CTF}A\left(\bar{T}_{w,CTF} - \bar{T}_{f,CTF}\right)$$

where h_{STAR} and h_{CTF} are the heat transfer coefficients in STAR and CTF respectively, A is the heat transfer area, $\bar{T}_{w,STAR}$ and $\bar{T}_{w,CTF}$ are the average wall temperatures in STAR and CTF respectively, and $\bar{T}_{f,STAR}$ and $\bar{T}_{f,CTF}$ are the average bulk fluid temperatures in the subchannel. Applying the assumption that the average bulk fluid temperature in each subchannel is equal between STAR and CTF, a multiplier between STAR and CTF can be defined as:

$$M = \frac{h_{STAR}}{h_{CTF}} = \frac{\left(\bar{T}_{w,CTF} - \bar{T}_f\right)}{\left(\bar{T}_{w,STAR} - \bar{T}_f\right)}$$

While M can be physically interpreted as the ratio of heat transfer coefficients between codes, for the surface mapping model it was expressed as a first order Taylor series dependent on the CTF mesh coordinates (θ and z). The first order Taylor series takes the form:

$$M(\theta, z) = M_o + \frac{\delta M(\theta, z)}{\delta \theta}(\theta - \theta_o) + \frac{\delta M(\theta, z)}{\delta z}(z - z_o)$$

or

$$M(\theta, z) = M_0 + M_{10}(\theta - \theta_o) + M_{20}(z - z_o)$$

where M_0 is a constant, M_{10} is a coefficient describing the linear azimuthal dependence, $(\theta - \theta_o)$ is the difference between a given θ value and the azimuthal reference point ($\theta_o = 0\ radians$), M_{20} is a coefficient describing the linear axial dependence, and $(z - z_o)$ is the difference between an axial position and the axial reference point ($z_o = initial\ z$). A graphical representation of the change in θ and change in z terms is given in Figure 1. Note that regardless of problem geometry, CTF resolution in the azimuthal direction is always 4 quadrants.

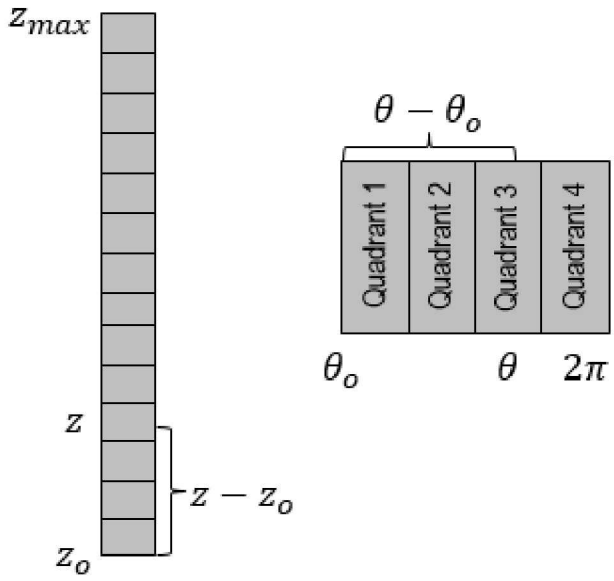

Figure 1: A graphical explanation of z-z_o and $\theta - \theta_o$ for any given z less than z_{max} and 2π respectively. Regardless of specified geometry, CTF always outputs rod values in terms of four quadrants.

2.1.2 Derivation of the Linear Average Surface Mapping Model

The average surface mapping model applies the multiplier, M, to CTF pre-generated surface wall temperatures to obtain CTF post-processed wall temperatures that are as close as possible to STAR surface wall temperatures. The average surface mapping model is based on the following relationship:

$$q^{"} = h\left(T_w - T_f\right)$$

where $q^{"}$ is heat flux, h is heat transfer coefficient, and $T_w - T_f$ is the difference between the rod wall temperature and the fluid temperature. It is assumed that the heat flux and average bulk fluid temperature in CTF and STAR would be the same for the same boundary conditions,

$$q^{"}_{CTF} = q^{"}_{STAR} = q^{"}$$
$$\bar{T}_{f,STAR} = \bar{T}_{f,CTF} = \bar{T}_f$$

thus, the calculated heat transfer based on the heat flux boundary condition and average temperatures out of CTF is:

$$h_{CTF-pre} = \frac{q^{"}}{\bar{T}_{w,CTF-pre} - \bar{T}_f}$$

where $h_{CTF-pre}$ is a result of temperatures taken from CTF output before the mapping model has been applied. With a calculated $h_{CTF-pre}$, the average surface mapping model can be expressed as:

$$\bar{T}_{w,CTF-post} = \frac{q^{"}}{M * h_{CTF-pre}} + \bar{T}_f$$

$$\bar{T}_{w,CTF-post} = \frac{q^{"}}{\left(M_0 + M_{10}(\theta - \theta_o) + M_{20}(z - z_o)\right) * h_{CTF-pre}} + \bar{T}_f$$

where $\bar{T}_{w,CTF-post}$ is the post-processed result of applying the multiplier to the CTF code output. The following residual is evaluated throughout this milestone to determine the effectiveness of the multiplier at mapping average surface temperatures from STAR to CTF.

$$Residual = \left|\bar{T}_{w,CTF-post} - \bar{T}_{w,STAR}\right|$$

3. SURFACE MAP MODEL VERIFICATION

Before calibrating the multiplier coefficients for a single channel demonstration problem, a verification analysis was performed on the average surface map model to ensure the model performs as expected. The verification analysis included finding an analytical solution for M, generating synthetic data to be used to plot the effect of the multiplier in MATLAB, and using the generated data to perform a calibration in Dakota using python.

3.1 Analytical Solution for M

The first step of the verification process was to find an analytical solution for the multiplier, M, based on a manufactured solution. As stated in 2.1.1, the physical interpretation of M is the following:

$$M = \frac{h_{STAR}}{h_{CTF}} = \frac{\left(\bar{T}_{w,CTF} - \bar{T}_{f,CTF}\right)}{\left(\bar{T}_{w,STAR} - \bar{T}_{f,STAR}\right)}$$

where it is possible to rewrite M in terms of the manufactured solution and assumptions. With $\bar{T}_{w,STAR}$ known and three equations,

$$\bar{T}_{f,STAR,MMS} = \bar{T}_{f,CTF,MMS} = \bar{T}_{f,MMS}$$

$$\bar{T}_{w,CTF,MMS} = \bar{T}_{w,STAR,MMS} + \Delta\bar{T}$$

$$\Delta\bar{T} = m_o^* + m_1^*(\theta - \theta_o) + m_2^*(z - z_o)$$

M becomes:

$$M_{exact,MMS} = \frac{\left((\bar{T}_{w,STAR,MMS} + \Delta\bar{T}) - \bar{T}_{f,MMS}\right)}{\left(\bar{T}_{w,STAR,MMS} - \bar{T}_{f,MMS}\right)}$$

$$M_{exact,MMS} = \frac{\left(\bar{T}_{w,STAR,MMS} + m_o^* + m_1^*(\theta - \theta_o) + m_2^*(z - z_o)\right) - \bar{T}_{f,MMS}}{\bar{T}_{w,STAR,MMS} - \bar{T}_{f,MMS}}$$

where m_o^*, m_1^*, and m_2^* are user-defined inputs to generate a manufactured solution. The subscript MMS denotes the quantities that are either manufactured or a result of the manufactured solution. This form of the exact solution is not useful when verifying the calibration of the average surface mapping model. Partial derivatives of $M_{exact,mms}$ are taken to obtain the coefficients of the first order Taylor series form of M. By setting $(\theta - \theta_o)$ and $(z - z_o)$ to zero, the analytical solution for M_o is:

$$M_{o,exact,MMS} = \frac{\bar{T}_{w,STAR,MMS} + m_o^* - \bar{T}_{f,MMS}}{\bar{T}_{w,STAR,MMS} - \bar{T}_{f,MMS}}$$

$$M_{o,exact,MMS} = 1 + \frac{m_o^*}{\bar{T}_{w,STAR,MMS} - \bar{T}_{f,MMS}}$$

where $M_{o,exact,MMS}$ is the analytical solution for the M_o coefficient in the first order Taylor series form of M. The partial derivative of $M_{exact,MMS}$ with respect to $(\theta - \theta_o)$ yields:

$$M_{10,exact,MMS} = \frac{\delta M}{\delta(\theta - \theta_o)} = \frac{m_1^*}{\bar{T}_{w,STAR,MMS} - \bar{T}_{f,MMS}}$$

where $M_{10,exact,MMS}$ is the analytical solution for the M_{10} coefficient in the first order Taylor series form of M. Taking the partial derivative of $M_{exact,MMS}$ with respect to $(z - z_o)$ produces:

$$M_{20,exact,MMS} = \frac{\delta M}{\delta(z - z_o)} = \frac{m_2^*}{\bar{T}_{w,STAR,MMS} - \bar{T}_{f,MMS}}$$

where $M_{20,exact,MMS}$ is the analytical solution for the M_{20} coefficient in the first order Taylor series form of M. Plugging in the analytical solutions for each coefficient gives a complete analytical solution for the first order Taylor series for M.

$$M_{exact,MMS} = M_{o,exact,MMS} + M_{10,exact,MMS}(\theta - \theta_o) + M_{20,exact,MMS}(z - z_o)$$

$$M_{exact,MMS} = 1 + \frac{m_o^*}{\bar{T}_{w,STAR,MMS} - \bar{T}_{f,MMS}} + \frac{m_1^*(\theta - \theta_o)}{\bar{T}_{w,STAR,MMS} - \bar{T}_{f,MMS}} + \frac{m_2^*(z - z_o)}{\bar{T}_{w,STAR,MMS} - \bar{T}_{f,MMS}}$$

$$M_{exact,MMS} = 1 + \frac{m_o^* + m_1^*(\theta - \theta_o) + m_2^*(z - z_o)}{\bar{T}_{w,STAR,MMS} - \bar{T}_{f,MMS}}$$

3.1.1 Analytical Solution for M with Noise

The same process can be followed to determine the analytical solution for M if random noise was introduced into the manufactured solution. For the purposes of this verification exercise, the noise was added to $\Delta\bar{T}$ such that:

$$\Delta\bar{T}_{noise} = m_o^* + m_1^*(\theta - \theta_o) + m_2^*(z - z_o) + rand * \left[\frac{1}{10}(max\Delta\bar{T})\right]$$

where the noise is defined as a random number multiplied by a tenth of the maximum $\Delta\bar{T}$. With this definition, the analytical solution for M using a manufactured solution becomes:

$$M_{exact,MMS,noise} = \frac{\left(\bar{T}_{w,STAR,MMS} + m_o^* + m_1^*(\theta - \theta_o) + m_2^*(z - z_o) + rand\left[\frac{1}{10}(max\Delta\bar{T})\right]\right) - \bar{T}_{f,MMS}}{\bar{T}_{w,STAR,MMS} - \bar{T}_{f,MMS}}$$

and after the coefficients are found using partial derivatives, the first order Taylor series form of $M_{exact,MMS,noise}$ is:

$$M_{exact,MMS,noise} = 1 + \frac{m_o^* + rand\left[\frac{1}{10}(max\Delta\bar{T})\right]}{\bar{T}_{w,STAR,MMS} - \bar{T}_{f,MMS}} + \frac{m_1^*(\theta - \theta_o)}{\bar{T}_{w,STAR,MMS} - \bar{T}_{f,MMS}} + \frac{m_2^*(z - z_o)}{\bar{T}_{w,STAR,MMS} - \bar{T}_{f,MMS}}$$

$$M_{exact,MMS,noise} = 1 + \frac{m_o^* + rand\left[\frac{1}{10}(max\Delta\bar{T})\right] + m_1^*(\theta - \theta_o) + m_2^*(z - z_o)}{\bar{T}_{w,STAR,MMS} - \bar{T}_{f,MMS}}$$

3.2 Generation of Synthetic Verification Data

Synthetic verification data was generated and used to ensure the average surface mapping model worked as expected before calibration with real data from STAR and CTF. The synthetic data was generated using the following relationships/expressions:

$$\bar{T}_{f,STAR,MMS} = \bar{T}_{f,CTF,MMS} = \bar{T}_{f,MMS}$$

$$\bar{T}_{w,STAR} = \bar{T}_{w,STAR,MMS}$$

$$\Delta\bar{T} = m_o^* + m_1^*(\theta - \theta_o) + m_2^*(z - z_o)$$

$$\bar{T}_{w,CTF,MMS} = \bar{T}_{w,STAR,MMS} + \Delta\bar{T}$$

where m_o^*, m_1^*, and m_2^* are arbitrarily chosen ($\neq 1$) to generate the synthetic data such that an exact solution is known and evidence of the effect of various shapes of M in the calculation of the post-processed CTF average wall temperatures is verified. The number of permutations of m_o^*, m_1^*, and m_2^*

to achieve all possible shapes of M is six. Table 1 provides the six combinations used in this verification analysis.

Table 1: Arbitrarily chosen values for m_o^*, m_1^*, and m_2^* such that all possible shapes of M could be verified in the post-processed CTF average wall temperature.

	Eval 1	Eval 2	Eval 3	Eval 4	Eval 5	Eval 6
m_o^*	2	0	0	2	2	2
m_1^*	0	3	0	3	0	3
m_2^*	0	0	5	0	5	5

Note that the values of 2, 3, and 5 were arbitrarily chosen and have no physical meaning. Other values could have been chosen; the only stipulation was that m_o^*, m_1^*, and m_2^* could not be equal to one, otherwise the behavior of M could not be verified.

3.2.1 Basic Case: $\overline{T}_{w,STAR,MMS}$ = constant

A basic test was performed to verify the model for M had the appropriate shape based on the six evaluations. To ensure the shape of M is easily identifiable, the manufactured average wall temperature for STAR, the manufactured average fluid temperature, and the manufactured heat flux were set to constants values.

The $\overline{T}_{w,STAR,MMS}$, $\overline{T}_{f,MMS}$, and q''_{MMS} manufactured solutions chosen for the base case are:

$$\overline{T}_{w,STAR,MMS} = \begin{bmatrix} 500 & 500 & 500 & 500 \\ 500 & 500 & 500 & 500 \\ 500 & 500 & 500 & 500 \\ 500 & 500 & 500 & 500 \\ 500 & 500 & 500 & 500 \end{bmatrix} \text{K} \quad \overline{T}_{f,MMS} = \begin{bmatrix} 485 \\ 485 \\ 485 \\ 485 \\ 485 \end{bmatrix} \text{K} \quad q''_{MMS} = 500 \ \frac{kW}{m^2 K}$$

where a plot of $\overline{T}_{w,STAR,MMS}$ is provided in Figure 4 for reference.

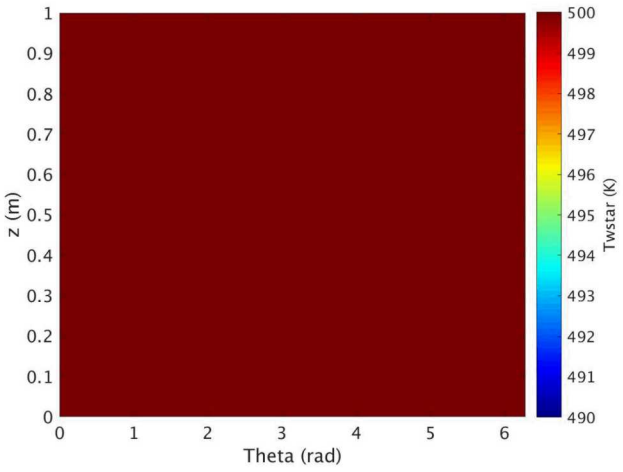

Figure 2: STAR manufactured average surface temperature used in base case verification of the shape of M.

The basic case manufactured solutions and each evaluation of m_0^*, m_1^*, and m_2^* were imported into a MATLAB version of the average surface mapping model to verify the shape of M. A colormap of M for each evaluation, at each azimuthal and axial position, is provided in Figure 3.

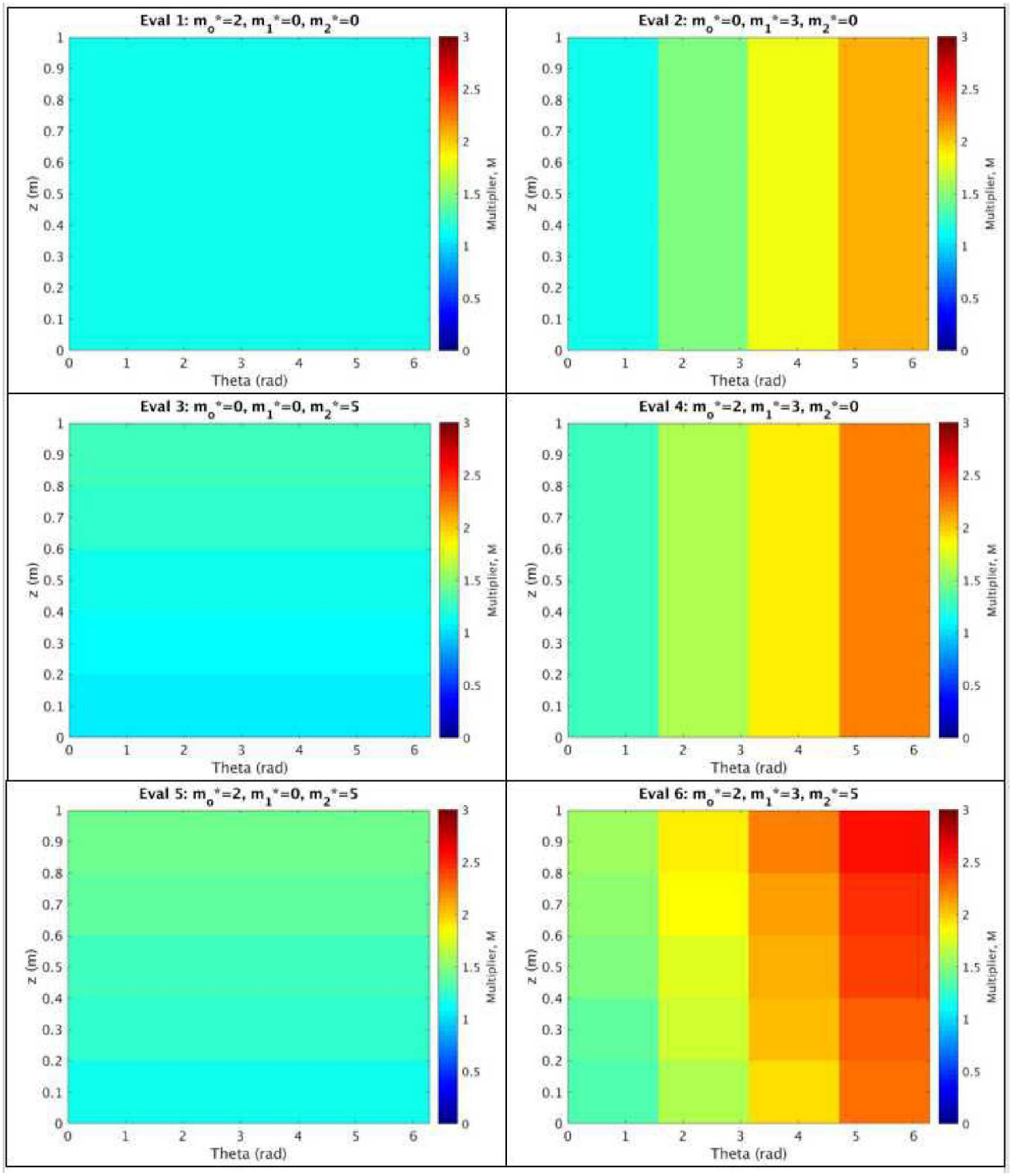

Figure 3: $M_{exact,MMS}$ at each azimuthal and axial position and for each evaluation of the base case manufactured solution. Note that the theta coordinate is divided into four segments in CTF.

The shape of M was as expected in each of the six evaluations using the constant manufactured solution. The expected shapes of M and the outcomes are provided in Table 2.

Table 2: Results of $M_{exact,MMS}$ for every evaluation of m_o^*, m_1^*, and m_2^* using the constant base case manufactured solution.

	Expected Shape of M	Resulting Shape of M as Expected?
Eval 1	Uniform across θ and z (M ≅ 1)	Yes
Eval 2	Variation in θ and uniform in z	Yes
Eval 3	Uniform in θ and variation in z	Yes
Eval 4	Similar to Eval 2, but $M_{Eval\ 4} > M_{Eval\ 2}$	Yes
Eval 5	Similar to Eval 3, but $M_{Eval\ 5} > M_{Eval\ 3}$	Yes
Eval 6	Variation in θ and z	Yes

3.2.2 Base Case with Added Complexity: $\bar{T}_{w,STAR,MMS} \neq$ constant

The base case in section 3.2.1 was used to ensure the appropriate shape behavior of M, but a more complex version of the base case is needed to verify the calibration process. A checkerboard pattern was chosen for $\bar{T}_{w,STAR,MMS}$ to increase the complexity, but retain debugging simplicity.

The $\bar{T}_{w,STAR,MMS}$, $\bar{T}_{f,MMS}$, and q''_{MMS} manufactured solutions chosen for the base case with added complexity are:

$$\bar{T}_{w,STAR,MMS} = \begin{bmatrix} 500 & 490 & 500 & 490 \\ 490 & 500 & 490 & 500 \\ 500 & 490 & 500 & 490 \\ 490 & 500 & 490 & 500 \\ 500 & 490 & 500 & 490 \end{bmatrix} \text{K} \quad \bar{T}_{f,MMS} = \begin{bmatrix} 485 \\ 485 \\ 485 \\ 485 \\ 485 \end{bmatrix} \text{K} \quad q''_{MMS} = 500\ \frac{kW}{m^2K}$$

where $\bar{T}_{w,STAR,MMS}$ resembles a checker board pattern and $\bar{T}_{f,MMS}$ and q''_{MMS} are constant for verification simplicity. A plot of $\bar{T}_{w,STAR,MMS}$ is provided in Figure 4 for reference.

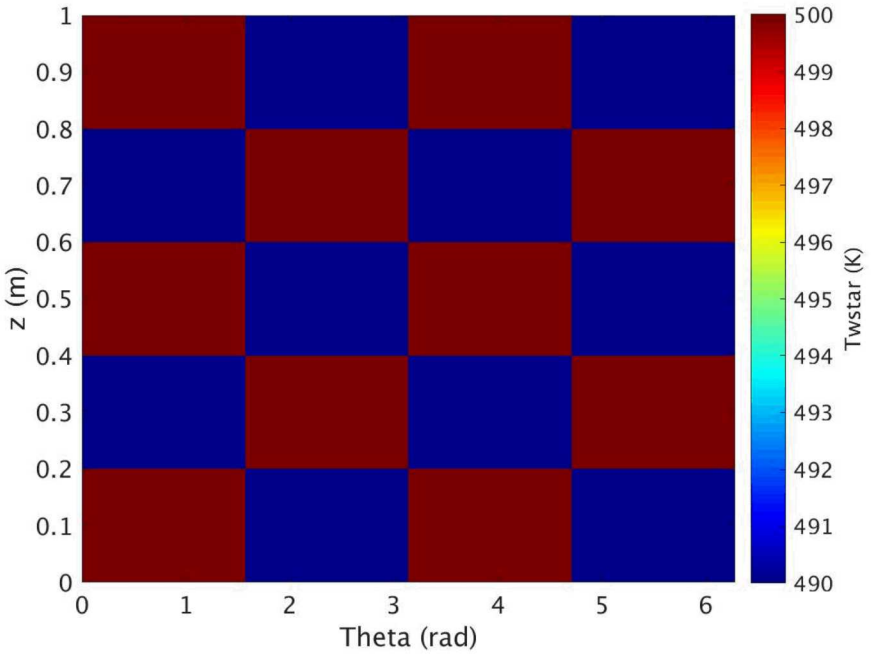

Figure 4: STAR manufactured average surface temperature used in verification analysis.

As in section 3.2.1, the manufactured solutions and each evaluation of m_o^*, m_1^*, and m_2^* were imported into a MATLAB version of the average surface mapping model to verify the shape of M. A colormap of M for each evaluation and each azimuthal and axial position is provided in Figure 5.

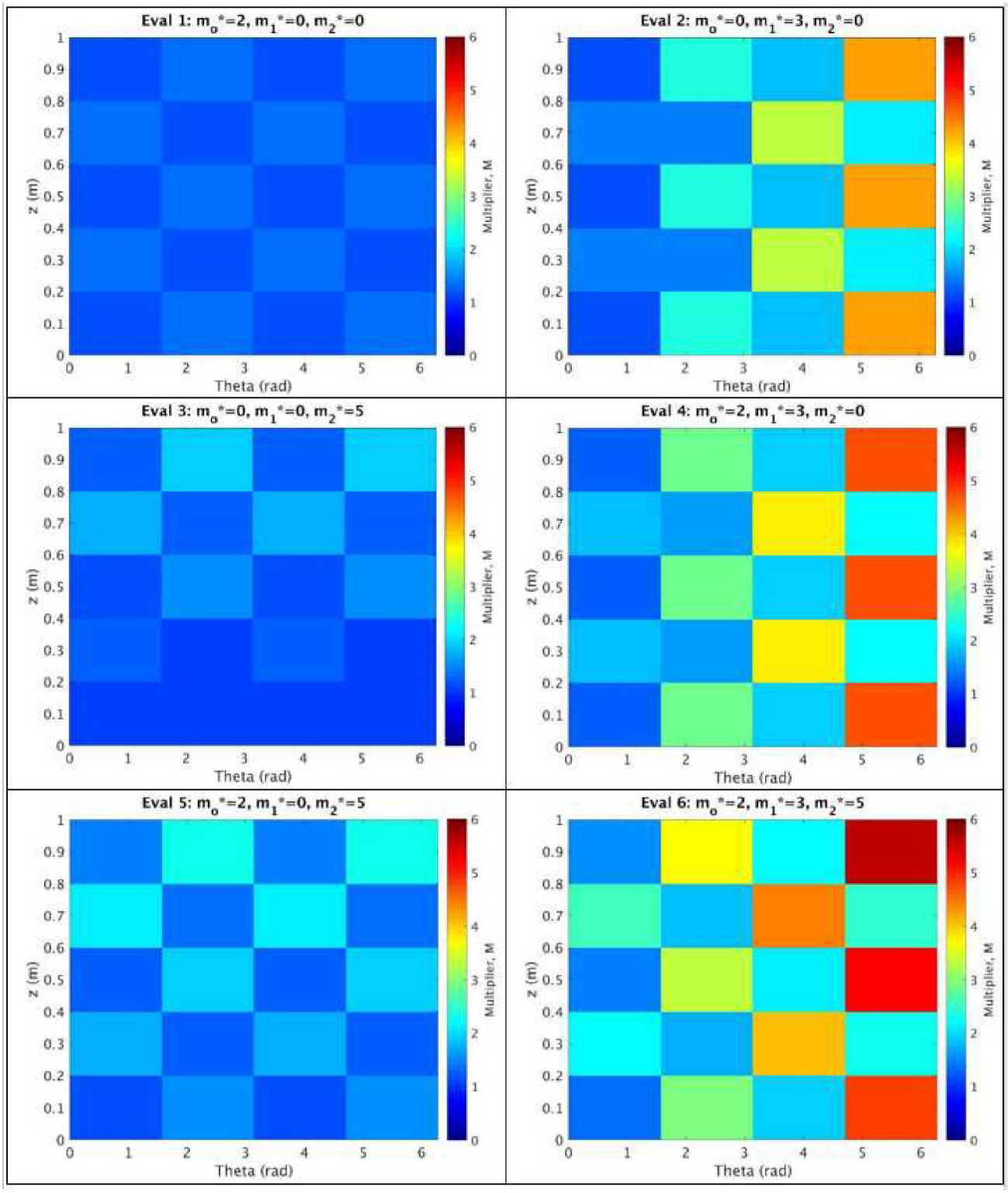

Figure 5: $M_{exact,MMS}$ at each azimuthal and axial position and for each evaluation.

The shape of $M_{exact,MMS}$ was as expected for each of the six evaluations in Figure 5 given that $\bar{T}_{w,STAR,MMS}$ has a checkerboard pattern. Since a multiplier is being applied, the low values of the checkerboard should remain lower than the higher values. The shape of M for every evaluation is not

as obvious for the checkerboard pattern, thus, Table 3 provides the results for each of the six evaluations.

Table 3: Results of $M_{exact,MMS}$ for every evaluation of m_o^*, m_1^*, and m_2^*.

	Expected Shape of M	Resulting Shape of M as Expected?
Eval 1	Uniform across θ and z (Retaining balanced checkerboard pattern)	Yes
Eval 2	Variation in θ and uniform in z	Yes
Eval 3	Uniform in θ and variation in z	Yes
Eval 4	Similar to Eval 2, but $M_{Eval\ 4} > M_{Eval\ 2}$	Yes
Eval 5	Similar to Eval 3, but $M_{Eval\ 5} > M_{Eval\ 3}$	Yes
Eval 6	Variation in θ and z	Yes

The base case with added complexity manufactured solution will be used to in the next section to verify the average surface mapping model calibration.

3.3 Verification Calibration

The verification calibration of the surface mapping model was tested three different ways: calibration to one manufactured dataset that did not contain noise; calibration to one manufactured dataset with noise; and calibration to 21 manufactured datasets with noise. The calibration was performed using the NL2SOL method in Dakota 6.7. NL2SOL is a deterministic calibration method that returns the optimal value and confidence interval associated with each calibration parameter.

Each test was based on the manufactured solution in section 3.2.2 with varying degrees of complexity. The values for m_o^*, m_1^*, and m_2^*, used to generate the manufactured solution, are the same as in evaluation 6 ($m_o^* = 2$, $m_1^* = 3$, and $m_2^* = 5$).

3.3.1 Test 1: One Dataset Without Noise

The first test utilized the manufactured solution from section 3.2.2 to explicitly perform a calibration to one dataset that does not contain noise. The purpose of this exercise was to ensure the calibration machinery was setup correctly. The initial point for the three calibration parameters was set to 0.1 to test the NL2SOL method's ability to identify an appropriate value for each parameter (which is somewhere around $M_0 \cong 1$, $M_{10} \cong 0.5$, and $M_{20} \cong 0.3$). Table 4 provides the summary of the first verification calibration test.

Table 4: Results of NL2SOL calibration of M_0, M_{10}, and M_{20} in Dakota 6.7 using one manufactured dataset without noise. CI stands for confidence interval and σ is standard deviation.

	Initial (Pre- Calibration)	Optimal (Post-Calibration)	Lower CI	Upper CI	σ
M_0	0.1	1.1016	0.4537	1.7494	0.6479
M_{10}	0.1	0.3067	0.1281	0.4853	0.1786
M_{20}	0.1	0.4457	-0.4974	1.3888	0.9431

The NL2Sol method provides the analyst with a confidence interval on the optimal values of each calibration parameter. These are given for each of the coefficients of M in Table 4, as well as the

standard deviation that is based on this interval. A graphical representation of Table 4 is given in Figure 6, where the bar represents the optimal value of each coefficient and the standard deviation is displayed using error bars.

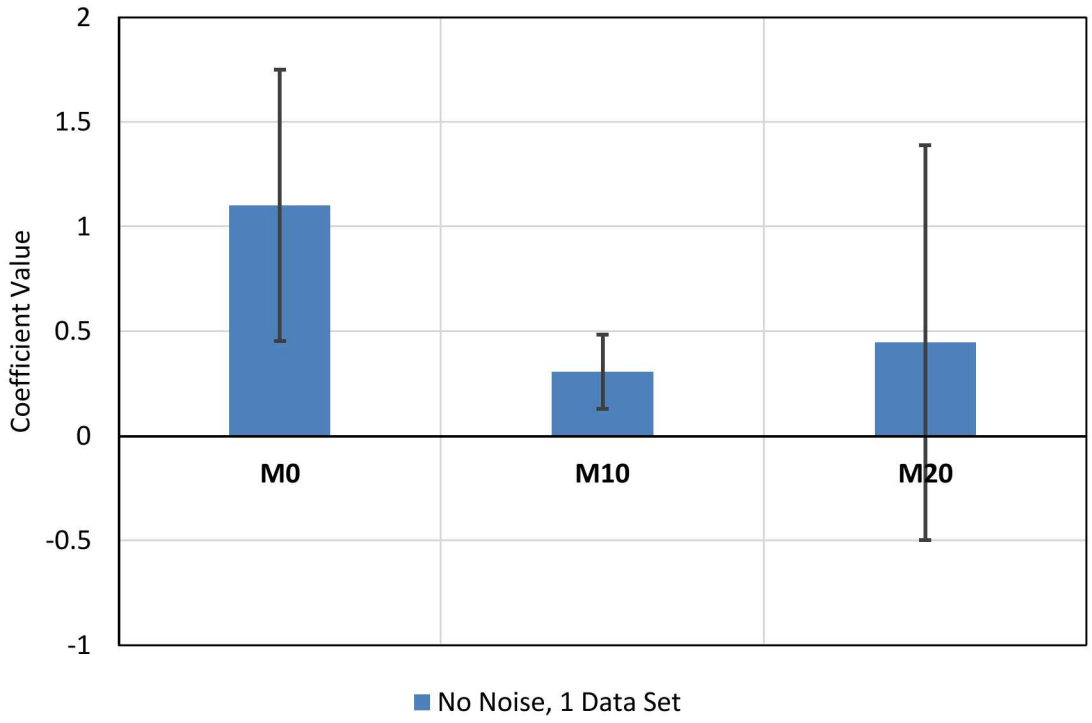

Figure 6: Graphical representation of the optimal values and standard deviation for the M coefficients based on a calibration of one manufactured dataset without noise.

The response functions returned to Dakota are the differences between CTF-post, the CTF wall temperature after the multiplier has been applied, and the manufactured STAR wall temperature ($Residual = \left|\bar{T}_{w,CTF-post} - \bar{T}_{w,STAR,MMS}\right|$). With each evaluation, Dakota suggests values for the calibration parameters to minimize or drive this residual to zero. Since the values of the calibrated M coefficients do not carry much physical meaning, the residual of $\left|\bar{T}_{w,CTF-post} - \bar{T}_{w,STAR,MMS}\right|$ was plotted based on the initial values for M_0, M_{10}, and M_{20} as well as the optimal values for the M coefficients in Figure 7.

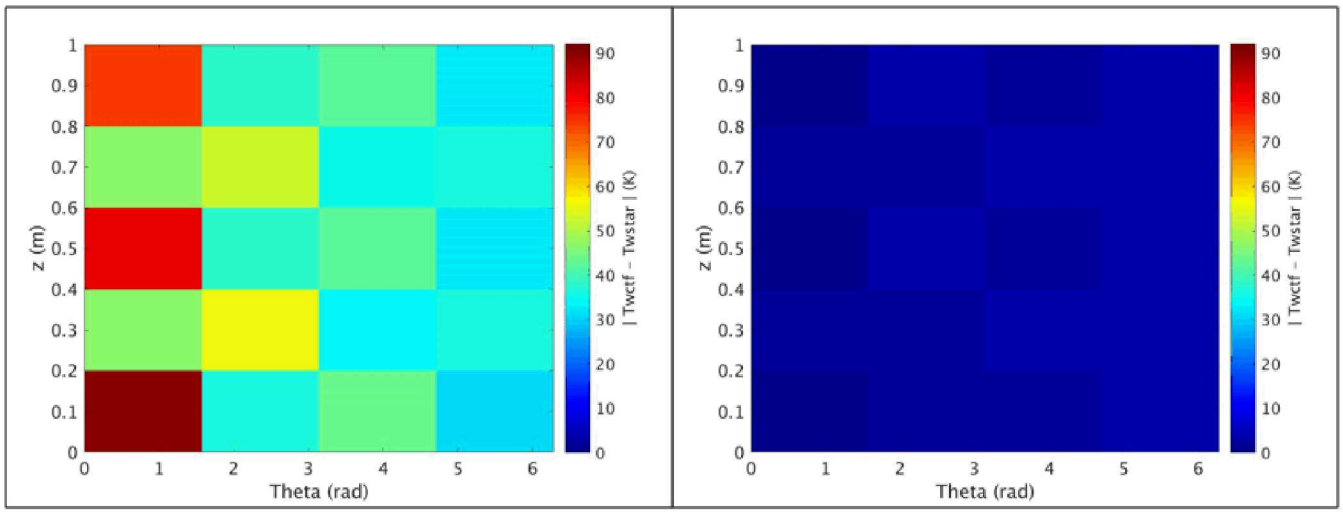

Figure 7: $\left|\bar{T}_{w,CTF-post} - \bar{T}_{w,STAR,MMS}\right|$ plotted before calibration (left) and $\left|\bar{T}_{w,CTF-post} - \bar{T}_{w,STAR,MMS}\right|$ plotted after calibration (right) for one manufactured dataset without noise.

As evident in Figure 7, values for $\bar{T}_{w,CTF-post}$ across the entire unrolled rod are much closer to values of $\bar{T}_{w,STAR,MMS}$. Note that both plots are on the same scale to denote the reduction in the residual between STAR and CTF with a calibrated multiplier. The largest residual value after calibration was within 4 K.

3.3.2 Test 2: One Dataset with Noise

The second test utilized the manufactured solution from section 3.2.2, but added noise to the $\Delta\bar{T}$ term (see section 3.1.1) to study the effects of a noisy solution on the average surface mapping multiplier model calibration. The same calibration process was followed as in section 3.3.1, since this test only utilized one manufactured dataset. The results of the calibration with noise are given in Table 5.

Table 5: Results of NL2SOL calibration of M_0, M_{10}, and M_{20} in Dakota 6.7 using one manufactured dataset with noise. CI stands for confidence interval and σ is standard deviation.

	Initial (Pre- Calibration)	Optimal (Post-Calibration)	Lower CI	Upper CI	σ
M_0	0.1	1.1072	0.4502	1.7641	0.6570
M_{10}	0.1	0.3077	0.1268	0.4887	0.1809
M_{20}	0.1	0.4468	-0.5092	1.4029	0.9560

The optimal values and confidence intervals for the M coefficients were approximately the same when noise was applied to $\bar{T}_{w,CTF,MMS}$. The similarities between test 1 and 2 are evident in the plot of Table 5 given in Figure 8.

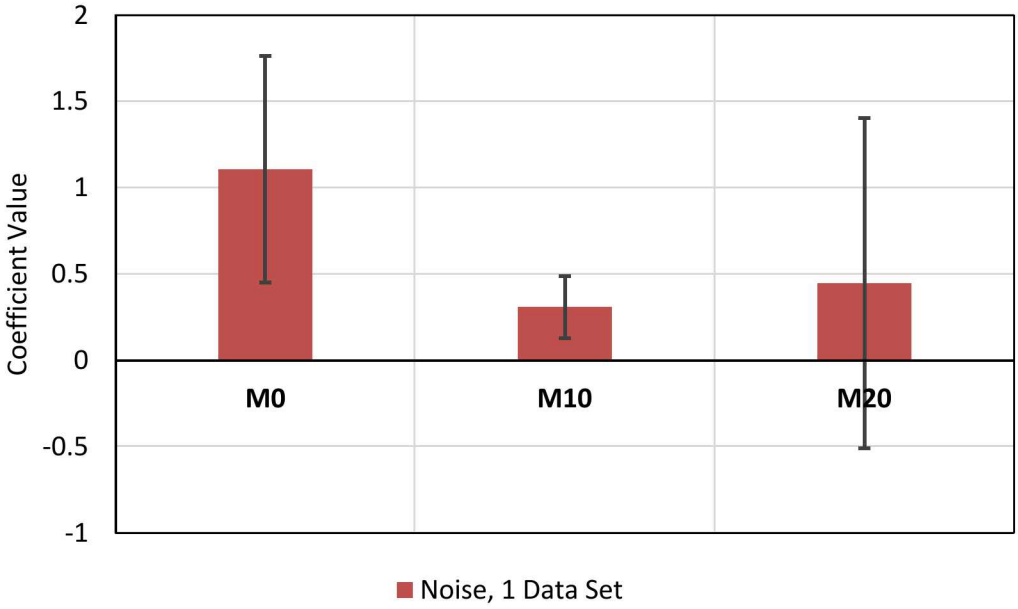

Figure 8: Graphical representation of the optimal values and standard deviation for the M coefficients based on a calibration of one manufactured dataset with noise.

The plot of $\left|\bar{T}_{w,CTF-post} - \bar{T}_{w,STAR,MMS}\right|$ using the calibrated values for the M coefficients is provided in Figure 9.

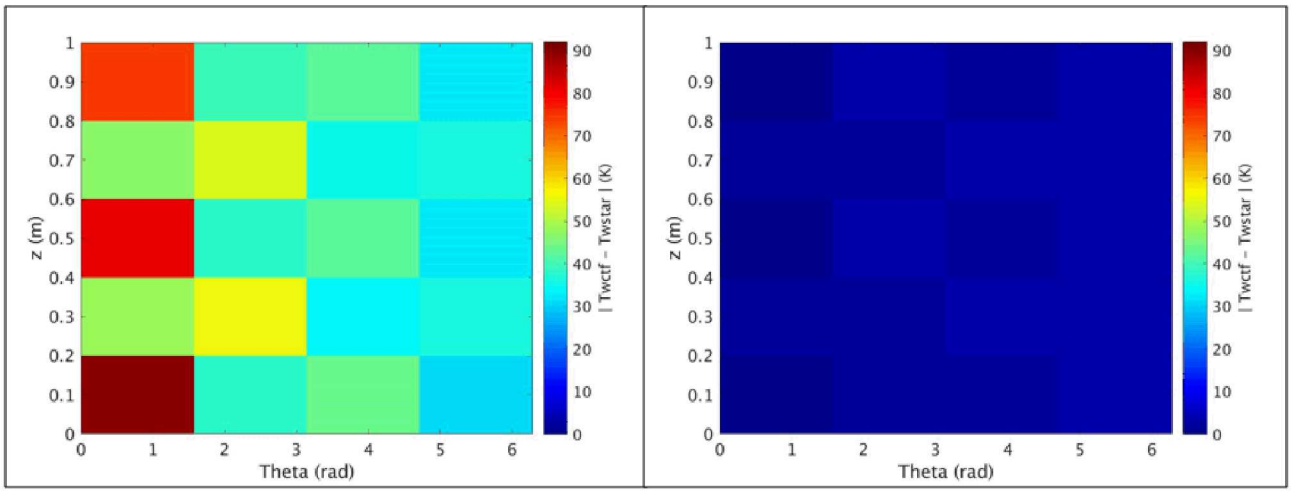

Figure 9: $\left|\bar{T}_{w,CTF-post} - \bar{T}_{w,STAR,MMS}\right|$ plotted before calibration (left) and $\left|\bar{T}_{w,CTF-post} - \bar{T}_{w,STAR,MMS}\right|$ plotted after calibration (right) for one manufactured dataset with noise.

The residual wall temperature values before and after the calibration are approximately the same as in section 3.3.1. The residual values are within 4 K as before. This indicates that a noise does not pose a problem to calibrating the multiplier in the average surface mapping model.

3.3.3 Test 3: Multiple Datasets with Noise

The third test utilized the manufactured solution from section 3.2.2 with noise as well as 20 other manufactured solutions of $\bar{T}_{w,CTF,MMS}$. The same initial points for the M coefficients were used and the results of the calibration are provided in Table 6.

Table 6: Results of NL2SOL calibration of M_0, M_{10}, and M_{20} in Dakota 6.7 using 21 manufactured datasets with noise. CI stands for confidence interval and σ is standard deviation.

	Initial (Pre- Calibration)	Optimal (Post-Calibration)	Lower CI	Upper CI	σ
M_0	0.1	1.1092	0.9861	1.2322	0.1231
M_{10}	0.1	0.3071	0.2733	0.3410	0.0339
M_{20}	0.1	0.4463	0.2673	0.6253	0.1790

The optimal values for M_0, M_{10}, and M_{20} are approximately the same as the other two tests, but the size of the confidence interval is much smaller (smaller standard deviation). A smaller confidence interval/standard deviation means that there is a higher confidence in the optimal values that were chosen by Dakota. The results are presented graphically in Figure 10.

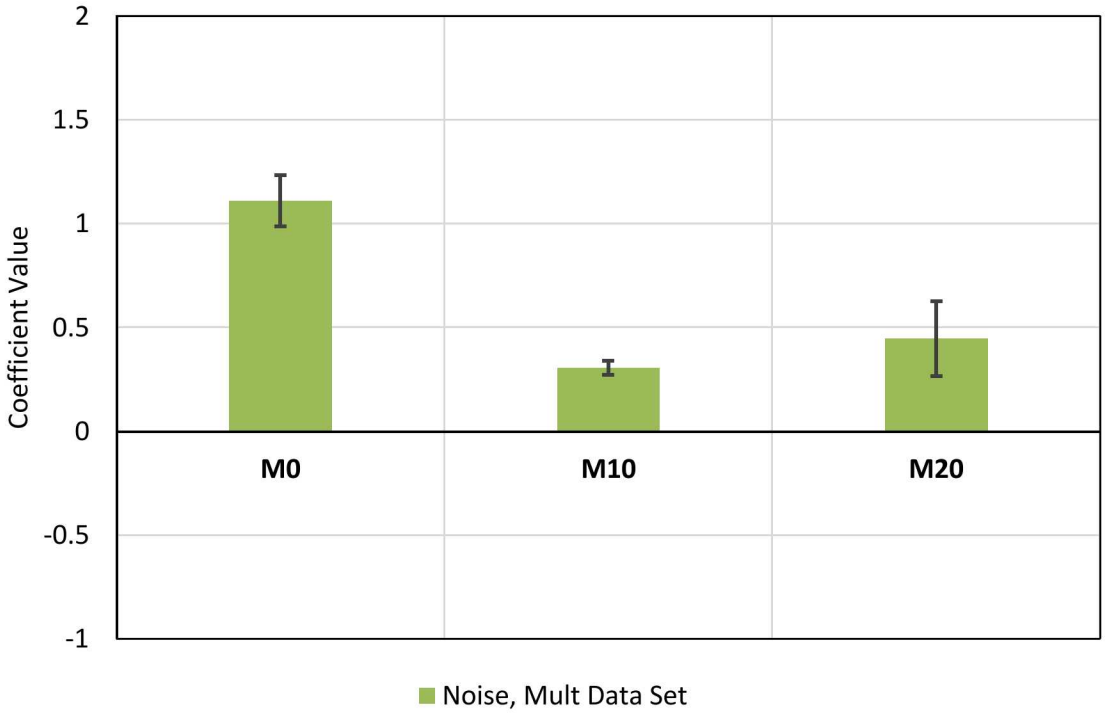

Figure 10: Graphical representation of the optimal values and standard deviation for the M coefficients based on a calibration of 21 manufactured datasets with noise. The confidence intervals are narrower since 21 sets of data were used to calibrate the three parameters.

In Figure 10, it is easier to see that the interval in which the optimal M coefficients exists is smaller, thus there is higher confidence in the Dakota-predicted values. The reduction in the confidence interval

is a direct result of using a larger dataset during the calibration process. With more data available, Dakota can improve the confidence in the optimal values.

The colormaps of before and after calibration of the multiplier coefficients are given in Figure 11.

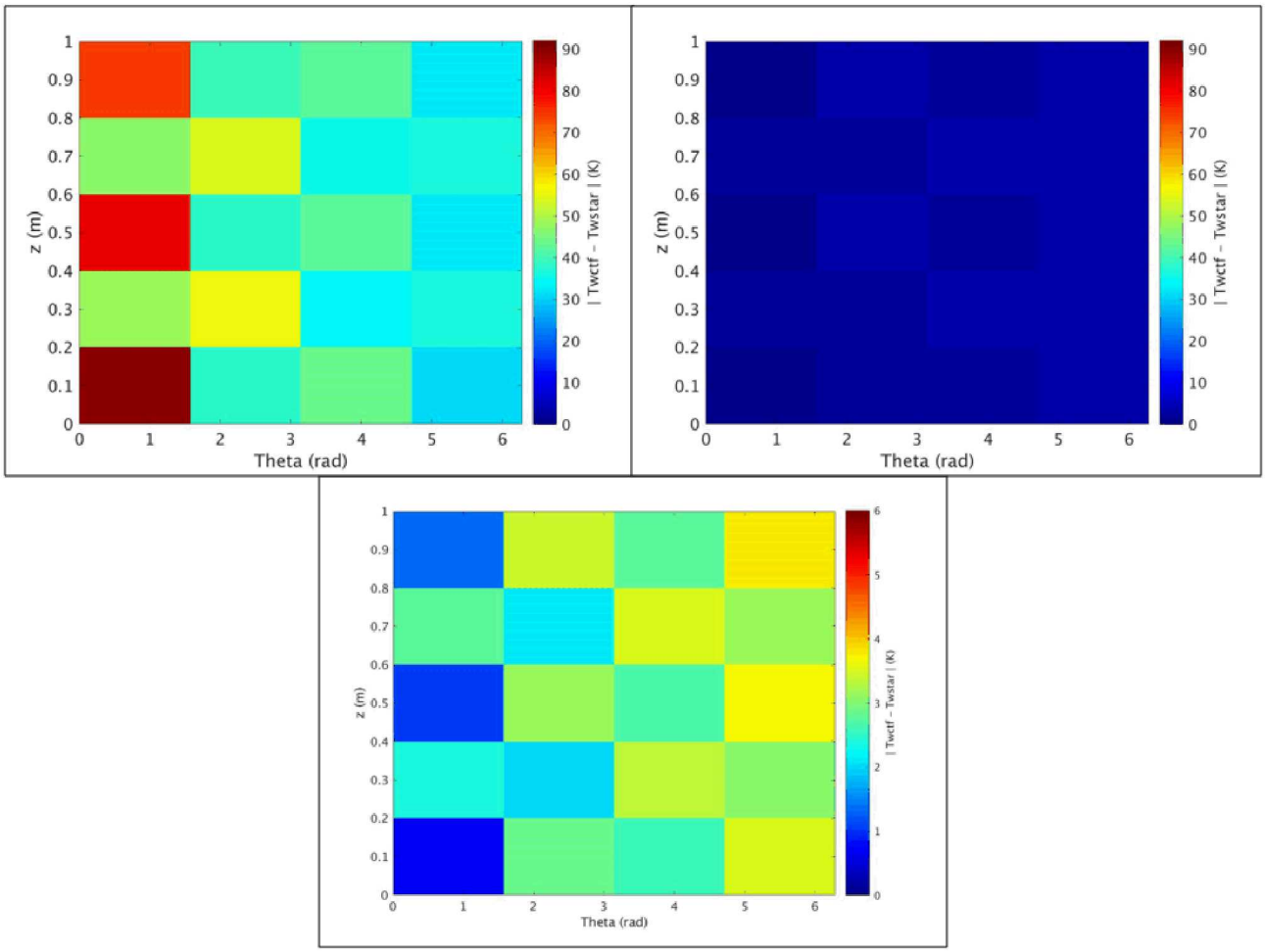

Figure 11: $\left|\overline{T}_{w,CTF-post} - \overline{T}_{w,STAR,MMS}\right|$ plotted before calibration (top left), $\left|\overline{T}_{w,CTF-post} - \overline{T}_{w,STAR,MMS}\right|$ plotted after calibration (top right), and $\left|\overline{T}_{w,CTF-post} - \overline{T}_{w,STAR,MMS}\right|$ plotted on a narrower scale (bottom) for 21 manufactured datasets with noise.

The top left and right colormaps of $\left|\overline{T}_{w,CTF-post} - \overline{T}_{w,STAR,MMS}\right|$ in Figure 11 are close to those presented for test 1 and 2 since the optimal values of the M coefficients are almost identical. The purpose of the plot added to the bottom of Figure 11 was to view the calibrated residual on a narrower scale. With the narrower scale, it is evident that the residual values are less than 4 K.

3.3.4 Verification Results

As stated in the previous sections, the Dakota-predicted optimal values for M_0, M_{10}, and M_{20} were approximately the same despite the addition of noise and added manufactured datasets. The lack of noticeable change in the optimal values of the calibration parameters is most likely due to the binary nature of the manufactured checkerboard STAR input wall temperatures. Without smooth data, it is

difficult to obtain values for the surface mapping model multiplier coefficients that work well for the entire domain.

The addition of noise to the wall temperatures widened the confidence intervals slightly, which is expected and more manufactured data did improve the confidence in the Dakota-predicted optimal multiplier coefficient values. Over 21 datasets, Dakota dramatically reduced the confidence intervals on M_0, M_{10}, and M_{20}, which was expected behavior. A summary of this improvement is provided in Figure 12.

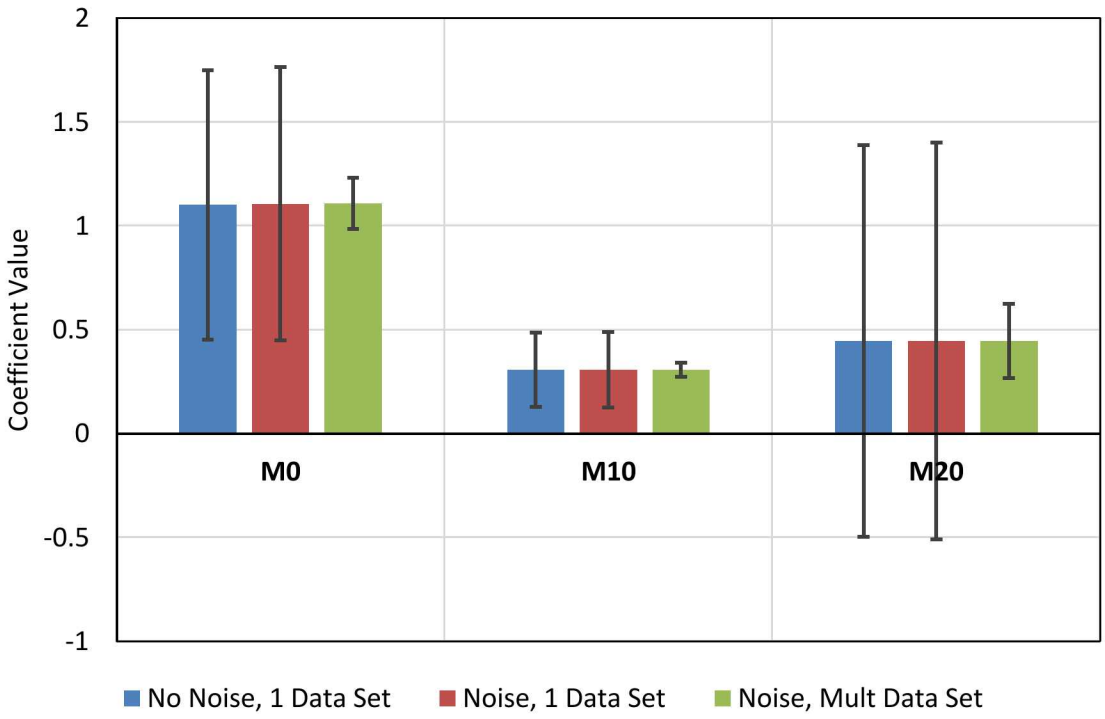

Figure 12: Graphical representation of the optimal values and standard deviation for the M coefficients based on each test calibration. While the optimal values for each coefficient are almost identical, the confidence intervals are slightly larger with the addition of noise and become very narrow with the addition of more data sets.

4. AVERAGE SURFACE MAP MODEL CALIBRATION

4.1 Demonstration Dataset

The dataset used to demonstrate the average surface mapping model was a simple single channel that is 1 m in length [1]. Only the top half of the single channel was modeled in STAR, thus this is the only region used during calibration. The top half of the geometry is divided into 20 axial regions, each with a height of 0.025 m. In STAR and CTF, a single channel is surrounded by 4 quarter rods, each with the same constant heat flux applied. A schematic of this geometry is pictured in Figure 13.

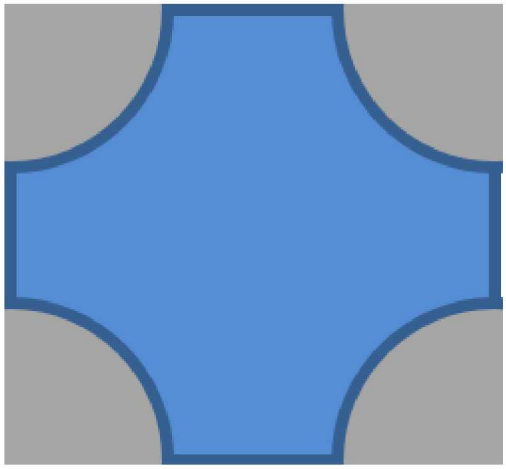

Figure 13: STAR and CTF geometry for the single channel problem. The four quarter rods are treated as if they are one single rod and have the same applied heat flux.

The single channel dataset consists of 22 cases, with case 0 representing nominal PWR conditions and the other cases being variations on the 3 nominal boundary conditions. The pressure for each test case is 155 bar. The boundary conditions for each case are given in Table 7.

Table 7: Boundary conditions for the single channel problem.

Case	T_{in} (K)	V_{in} (m/s)	q" (kW/m^2)
0	565.93	5.982	5.60104e+02
1	555.93	5.982	5.60104e+02
2	560.93	5.982	5.60104e+02
3	570.93	5.982	5.60104e+02
4	575.93	5.982	5.60104e+02
5	580.93	5.982	5.60104e+02
6	585.93	5.982	5.60104e+02
7	590.93	5.982	5.60104e+02
8	565.93	2.991	5.60104e+02
9	565.93	4.008	5.60104e+02
10	565.93	5.025	5.60104e+02
11	565.93	6.042	5.60104e+02
12	565.93	7.059	5.60104e+02
13	565.93	8.076	5.60104e+02
14	565.93	9.092	5.60104e+02
15	565.93	5.982	5.60104e+01
16	565.93	5.982	2.24042e+02
17	565.93	5.982	3.92073e+02
18	565.93	5.982	5.60104e+02
19	565.93	5.982	7.28136e+02
20	565.93	5.982	8.96167e+02
21	565.93	5.982	1.06420e+03

All 22 cases are used in the deterministic calibration of the average surface mapping model. For each case, note that only the top half of the domain was used (i.e. 0.5 m ≤ z ≥ 1 m).

4.2 Surface Map Deterministic Calibration using NL2SOL

A deterministic calibration using NL2SOL was performed using the single channel dataset after the average surface mapping model calibration framework was verified in section 3. The same NL2SOL calibration process as section 3.3.3 was used, but with a dataset that contains one more experiment and 20 axial levels (ranging from a z of 0.5 m to 1 m) compared to 5 axial levels in the verification problem. The results of the NL2SOL calibration are given in Table 8.

Table 8: Results of NL2SOL calibration of M_0, M_{10}, and M_{20} in Dakota 6.7 using 22 single channel datasets. CI stands for confidence interval and σ is standard deviation.

	Initial (Pre- Calibration)	Optimal (Post-Calibration)	Lower CI	Upper CI	σ
M_0	0.1	1.0837	1.0825	1.0850	0.0013
M_{10}	0.1	0.0021	0.0017	0.0025	0.0004
M_{20}	0.1	0.0438	0.0416	0.0460	0.0022

The optimal value for M_0 was close to the optimal value in the verification problem and in the range of what would be expected when $\bar{T}_{w,CTF-pre}$ is within 3 K of $\bar{T}_{w,STAR}$ for the entire dataset (every

azimuthal and z position for each test). The optimal values for M_{10} and M_{20} were much lower than the values seen in the verification problem. This behavior is anticipated given that there is very little change in the average wall temperature in the azimuthal direction (less than 0.1 K) and z direction (between 0.2 and 5.1 K depending on the experiment). A graphical representation of the NL2SOL calibration is provided in Figure 14.

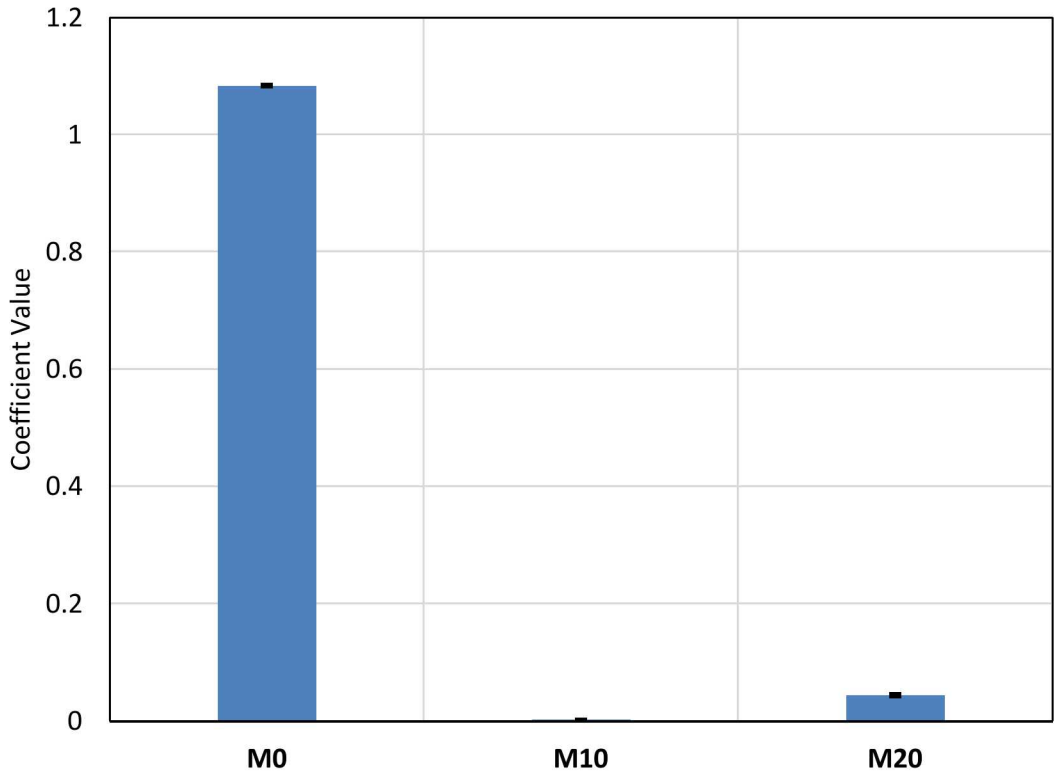

Figure 14: Graphical representation of the optimal values and standard deviation for the M coefficients from the NL2SOL calibration using the single channel data. With the use of 22 datasets in calibration, the confidence intervals became small enough that they are almost not visible in this figure.

In Figure 14 it is evident how small M_{10}, and M_{20} are in relation to M_{10} as stated when looking at the values in the previous paragraph. The confidence intervals on each of the coefficients of M are also much smaller than the verification problems because of the 22 datasets used in the calibration. The small confidence intervals are an indicator that Dakota is very confident in the optimal values based on the available data.

A colormap of $\left|\bar{T}_{w,CTF-post} - \bar{T}_{w,STAR}\right|$ for every experiment after calibration of the multiplier coefficients are given in Figure 15.

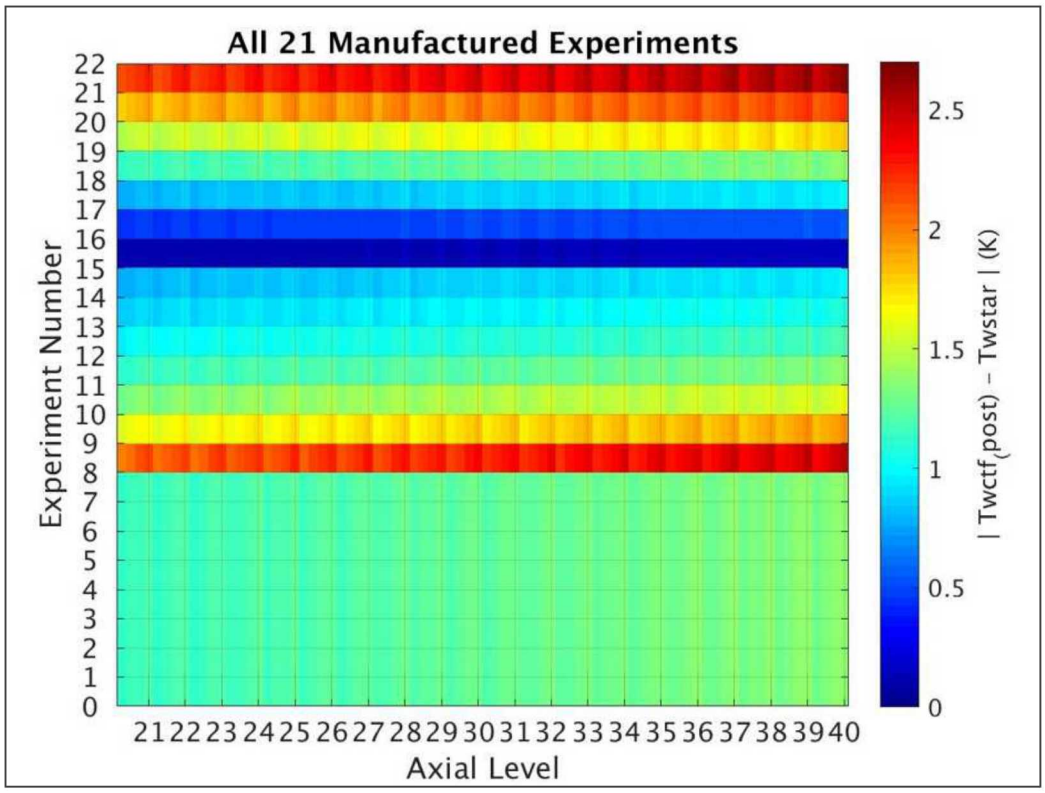

Figure 15: $\left|\overline{T}_{w,CTF-post} - \overline{T}_{w,STAR}\right|$ plotted after calibration for 22 single channel datasets. Each row represents one of the 22 experimental tests in array form (every 4 columns represents 2 pi in θ for each axial level).

In this figure, each y-axis row corresponds to one of the 22 experiments and each of the x-axis tick marks corresponds to an axial level. The first 8 experiments are about the same, approximately 1.25 K, but some of the experiments are closer to 2.5 (experiment 9 and 22) or 0.25 K (experiment 16 and 17). Overall, the calibrated coefficients for M produce a $\overline{T}_{w,CTF-post}$ that is within 2.5 K of $\overline{T}_{w,STAR}$. Colormaps for three of the test cases are given in Figure 16.

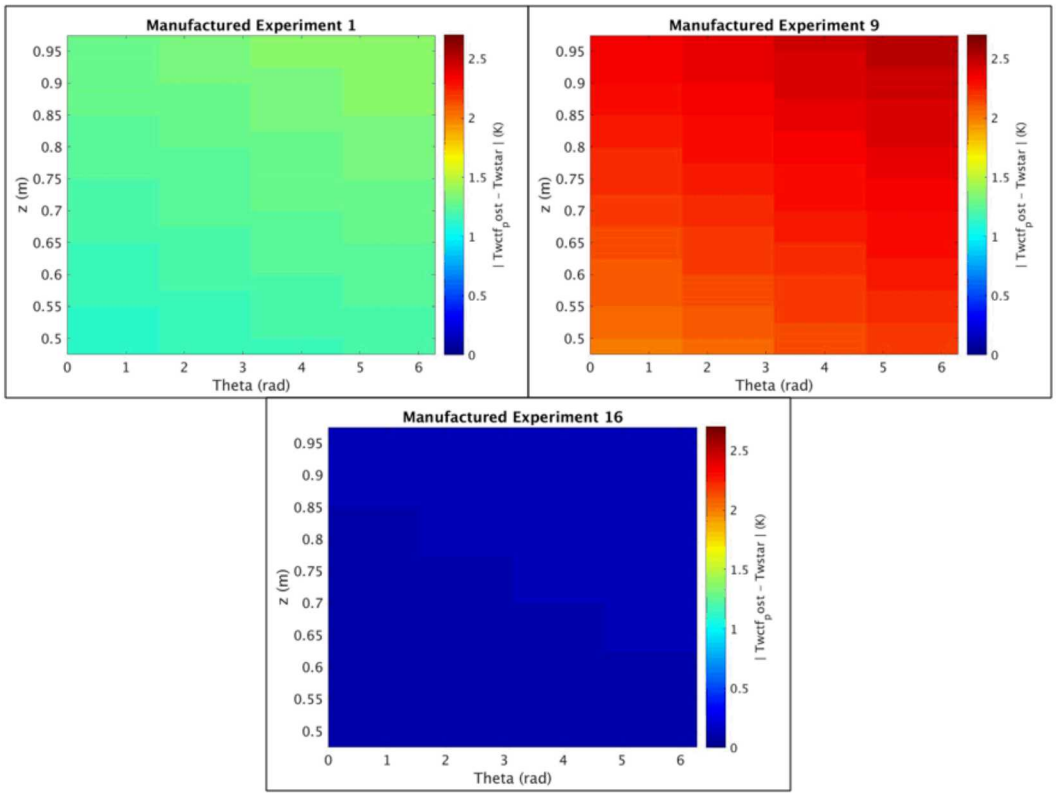

Figure 16: $\left|\overline{T}_{w,CTF-post} - \overline{T}_{w,STAR}\right|$ plotted after calibration for Experiment 1 (top left), $\left|\overline{T}_{w,CTF-post} - \overline{T}_{w,STAR}\right|$ plotted after calibration for Experiment 9 (top right), and $\left|\overline{T}_{w,CTF-post} - \overline{T}_{w,STAR}\right|$ plotted for Experiment 16 (bottom).

Figure 16 provides an example of tests that have a 1.25 K, 2.5 K, and 0.25 K difference between a $\overline{T}_{w,CTF-post}$ and $\overline{T}_{w,STAR}$ respectively. The structured versions of the colormaps for the experiments in Figure 15.

5. FUTURE WORK AND IMPROVEMENTS

The current average surface mapping model only incorporates azimuthal and axial dependence for a single rod. Future work for this model includes adding fluid property dependencies as well as expand the geometry dependencies to multiple rod geometries.

5.1 Fluid and Flow Property Dependence

Determining which fluid and flow properties to include in the average surface mapping model was the work of summer intern, Daniel Orea. As an exercise to understand which fluid and flow properties are of interest, Daniel derived an expression for wall temperature from the heat transfer rate equation:

$$\dot{Q}(z) = \dot{m}c_p \frac{dT_W}{dz}$$

$$\dot{m}c_p \frac{dT_W}{dz} = q'$$

$$\int_{T_{in}}^{T} dT_W = \frac{q'}{\dot{m}c_p} \int_{z_o}^{z} dz$$

$$T_W(z) = \frac{q'}{\dot{m}\, c_p}(z - z_o) + T_{in}$$

where $\dot{m}$ is mass flow rate, c_p is specific heat, and T_{in} is inlet temperature. Based on this derivation, the multiplier in the average surface mapping model should be dependent on position, mass flow rate, linear heat rate, and properties of the fluid.

The fluid and flow property dependence was defined in such a way that it would fit into the average surface mapping model work previously described in this milestone report. This is accomplished using the first order Taylor series approach to the multiplier, M:

$$M = M_0 + M_1\Delta\theta + M_2\Delta z$$

where M_1 and M_2 are functions of inlet conditions and fluid properties. The first order Taylor series of M_1 and M_2 is:

$$M_1 = M_{10} + \frac{\delta M}{\delta G}\Delta\dot{m} + \frac{\delta M}{\delta Re}\Delta Re + \frac{\delta M}{\delta Pr}\Delta Pr + \frac{\delta M}{\delta q'}\Delta q' + \frac{\delta M}{\delta T_{in}}\Delta T_{in}$$

$$M_2 = M_{20} + \frac{\delta M}{\delta G}\Delta\dot{m} + \frac{\delta M}{\delta Re}\Delta Re + \frac{\delta M}{\delta Pr}\Delta Pr + \frac{\delta M}{\delta q'}\Delta q' + \frac{\delta M}{\delta T_{in}}\Delta T_{in}$$

where $\dot{m}$ is mass flow rate, Re is Reynold's number, Pr is Prandtl number, and q is linear heat rate. The expressions for M_1 and M_2, that will be used in the average surface mapping model, are:

$$M_1 = M_{10} + M_{11}\Delta\dot{m} + M_{12}\Delta Re + M_{13}\Delta Pr + M_{14}\Delta q' + M_{15}\Delta T_{in}$$

$$M_2 = M_{20} + M_{21}\Delta\dot{m} + M_{22}\Delta Re + M_{23}\Delta Pr + M_{24}\Delta q' + M_{25}\Delta T_{in}$$

where M_{10} and M_{20} are defined the same as in section 2.1. The same calibration process would be followed, but many more sets of data would be needed beyond the 22 used in section 4, to calibrate 13 coefficients instead of the 3 coefficients calibrated in section 4.

5.2 Bayesian Calibration

A Bayesian calibration was not performed for this analysis due to time constraints. To complete the Bayesian process for the dataset described in section 4.1, some estimate of the error in the STAR

wall temperatures and additional data would be beneficial. The use of a surrogate is most likely not necessary given that the simulation in this example is a post-processing calculation in python, and does not require additional STAR or CTF runs beyond those used to populate the dataset.

A benefit of Bayesian calibration over deterministic calibration (used in section 4.2), is the use of mutual information to determine which STAR runs to perform. Mutual information tells the analyst where to focus on collecting more data, which will improve the calibration results by decreasing uncertainty as much as possible. Deterministic calibration with NL2SOL only yields confidence intervals, but Bayesian calibration yields a distribution.

5.3 Expanding to Larger Geometries

The single channel problem was used as a demonstration dataset for development and calibration of the multiplier in the average surface mapping model. Future work will include expanding the model to ultimately account for larger, more complex geometries, such as a fuel bundle with mixing vane grid spacers. Special attention will need to be devoted to determining how to incorporate mixing vane orientation dependence into the average surface temperature mapping model. Using a 5x5 mixing vane bundle dataset would be the next logical test problem for development of the average surface mapping model.

5.4 Incorporate into Surface Mapping Model

Once the average surface mapping model incorporates the dependencies of interest, it will be inserted into the surface mapping model developed by Lindsay Gilkey [2] and PHI. This model works by mapping fluctuations of surface temperatures from the average surface temperature. The average surface temperature will be supplied by the average surface mapping model described in this milestone report.

6. CONCLUSIONS

The coefficients in the average surface mapping model multiplier were successfully calibrated for axial and azimuthal dependence for a single channel problem. Overall, the calibration process and results were as expected and the confidence intervals on the calibrated coefficients were very narrow (standard deviation on the order of 0.001). Narrow confidence intervals denote high confidence in the optimal values of the coefficients that were determined through the deterministic calibration.

Future improvements to the average surface mapping model will be conducted in three steps. The first will be to incorporate fluid and flow property dependencies into the multiplier. This can be accomplished by adding these dependencies to the M_1 and M_2 coefficients as a first order Taylor series. This will apply the fluid and flow properties in the θ and z coordinates and result in approximately 13 multiplier coefficients. More data will be needed to effectively calibrate the new coefficients.

Improving the average surface mapping model will also occur through Bayesian calibration. Dakota will use Bayesian calibration to calculate the distribution on each of the multiplier coefficients, thus providing more information on the uncertainty in their value.

The third way the average surface mapping model will be improved is by adding geometric complexity. This will be accomplished by applying and calibrating the model to geometries such as 5x5 and 17x17 fuel bundles.

When appropriate after these modifications have been made, the average surface mapping model can be inserted into the surface mapping model developed by Lindsay Gilkey [2]. This will provide a better estimate of the average temperatures that will be used to determine the surface temperature fluctuation mapping.

LIST OF REFERENCES

[1] R. Salko, M. O. Delchini, L. Gilkey and D. Pointer, "CTF Heat Transfer Model Calibration Plan," February 2018.

[2] L. Gilkey, "Surface Temperature Mapping Models for STAR and CTF, L3: PHI.CTF.P17.02," 2018.